


RESEARCH ARTICLE

60-GHz Compact Vertically Polarized End-Fire Monopole-Based Yagi Antenna-in-Package for Wideband Mobile Communication

HONGYI KIM¹, TAE HWAN JANG¹, (Member, IEEE), AND CHUL SOON PARK¹, (Fellow, IEEE)

¹School of Electrical Engineering, Korea Advanced Institute of Science and Technology (KAIST), Daejeon 34141, South Korea

²School of Electronic Engineering, Hanyang University, Ansan 15588, South Korea

Corresponding author: Tae Hwan Jang (hundredwin@hanyang.ac.kr)

This work was supported in part by the Research Fund of Hanyang University under Grant HY-2022-2565; and in part by the Institute of Information and Communications Technology Planning and Evaluation (IITP) Grant through the Korea Government (MSIT), High-Resolution Vector Network Analyzer SW Development Supporting Sub-Thz Frequency Band, under Grant 2022-0-00859.

ABSTRACT In this work, 60-GHz wideband, compact vertically polarized end-fire monopole-based Yagi antenna-in-package is proposed for mobile devices. The antenna was arranged like a monopole array, and the size was minimized by utilizing the image effect. Advantages of the proposed antenna structure include reduction of bond-wire loss by inserting a cavity to make the antenna and chip the same height and size reduction due to image effect. For practical use, a proposed antenna is interconnected with CMOS chip via a bond-wire interconnect. The measured results show 4.99dBi peak gain with 3.5dB fluctuation within 60GHz unlicensed band. S_{11} bandwidth is 10.6GHz(57.6-67GHz) which corresponds to 16% fractional bandwidth. The total volume of the antenna is $0.74 \times 1.14 \times 0.15\lambda_0^3$.

INDEX TERMS Monopole antenna, Yagi-Uda antenna, 60GHz, wideband, antenna-in-package, mobile devices, LTCC.

I. INTRODUCTION


In 2001, the FCC allotted a continuous section of spectrum (57–66 GHz) for wireless communication in unlicensed usage [1]. Since the 60GHz unlicensed band has the widest frequency spectrum up to the 100GHz frequency band, high-speed communication using the wideband is possible. In fact, a communication link up to several tens of Gbps is realized in [2], [3], [4], and [5]. To cover the wide industrial, scientific, and medical (ISM) band of the 60-GHz unlicensed band spectrum, a radio is required to have a wideband antenna which covers from 57 GHz to 66 GHz. In order to apply the above frequency to mobile communication, a wideband antenna in package that radiates toward 3-axis(x-, y- and z-) is presented in [6], [7], and [8].

In case of the antenna in package for 3-axis radiation, the end-fire antenna must also be designed. The end-fire antennas for mobile devices are mainly realized in dipole

[9], [10], [11], [12], Yagi-Uda [13], [14], [15] and tapered [16], [17], [18] type, which polarization is horizontal. Not only horizontal polarization but also vertical polarization must be used at the same time for practical use, so an end-fire antenna with vertical polarization must also be used.

In [19], [20], [21], [22], and [23], a wideband vertically polarized end-fire antenna is presented. The multi-beam end-fire magneto-electric dipole antenna array for millimeter-wave applications is presented in [19], and H-plane sectoral post-wall horn antenna is presented in [20]. In [21], the antenna package provides the end-fire radiation from the open-ended post-wall waveguide built into the side of the package. The phase corrected H-plane horn antenna in gap SIW technology in [22].

Since the feeding network of these antennas is based on SIW(Substrate Integrated Waveguide), the overall size of the antenna is very bulky, so it is difficult to use directly in mobile devices. Therefore, compact antenna in package solution interconnecting RFIC is required.

The associate editor coordinating the review of this manuscript and approving it for publication was Tutku Karacolak¹.

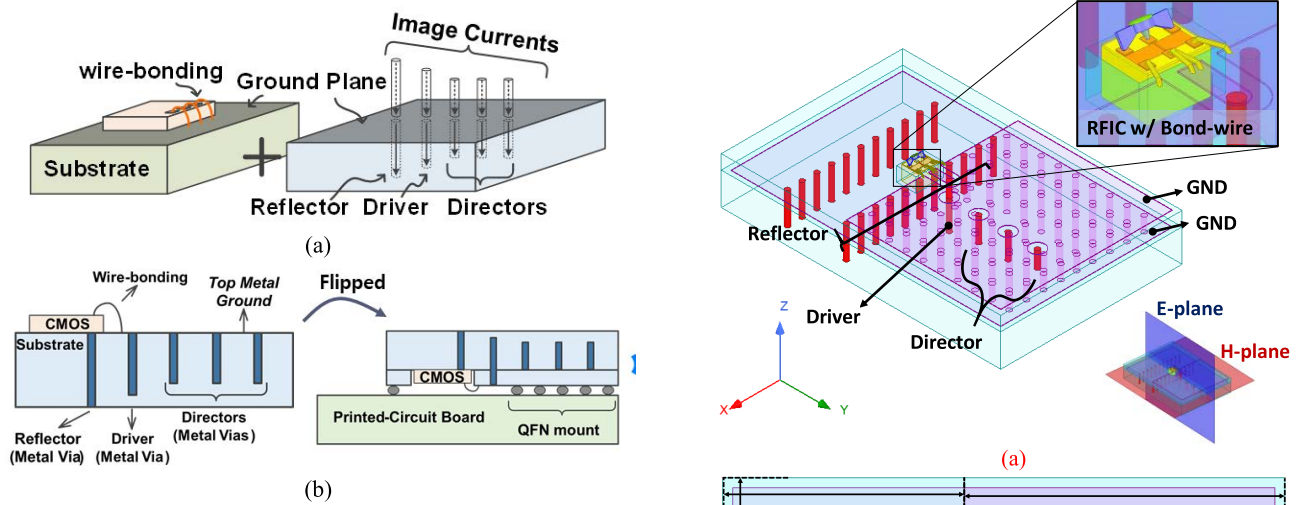


FIGURE 1. Proposed antenna design concept; (a) vertically polarized end-fire Antenna-in-Package integrated with CMOS RFIC and (b) QFN package with PCB base board.

In [23], vertically polarized end-fire planar folded slot antenna is proposed. Although microstrip line feeding is adopted to this antenna to reduce the size of the antenna, the fractional bandwidth is as low as 9.7%.

In [24], via-monopole based quasi Yagi-Uda antenna is proposed for W-band application. Although it has a monopole structure, since the antenna radiator is exposed to the air, there is a possibility that the radiation pattern is easily distorted by the components outside the antenna. In addition, the surface wave is severe by using a glass substrate with a dielectric constant of 4.6, but the antenna substrate and width are not optimized, so the radiation pattern is uneven even in the boresight direction. Moreover, the antenna is not designed considering the connection with the actual RFIC.

In [25], low-cost Yagi-Uda monopole array is presented. This antenna is implemented in the general cellular frequency band. It is expected that the radiation pattern will not be good due to the surface wave characteristics due to the dielectric constant of the substrate itself when it is implemented in the millimeter wave band.

In this work, vertically polarized monopole-based Yagi type antenna in package is proposed for mobile devices. Fig. 1 shows the proposed antenna design concept. A monopole driver is used as a radiator instead of a dipole driver to radiate the vertically polarized wave. The monopole driver is operated by an image effect as inserting a ground structure. Compared to the dipole antenna which requires an additional balun which is a single to differential converter, extra space for the balun isn't required so the antenna can be configured with a small area in case of monopole antenna.

The process of packaging the antenna with RFIC using wire-bonding is described. RFIC is placed on the metal ground plane to reduce interference with the inside of the substrate and secure the bottom ground of the CMOS IC in case of bond-wire packaging. As shown in Fig. 1 (b), a vertical Yagi-Uda antenna can be realized using QFN packaging

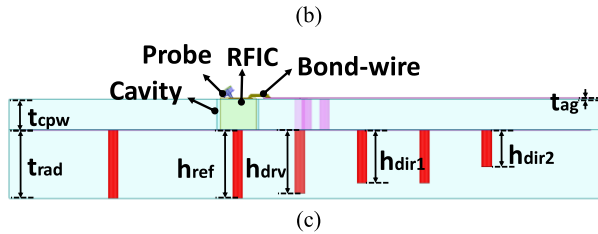
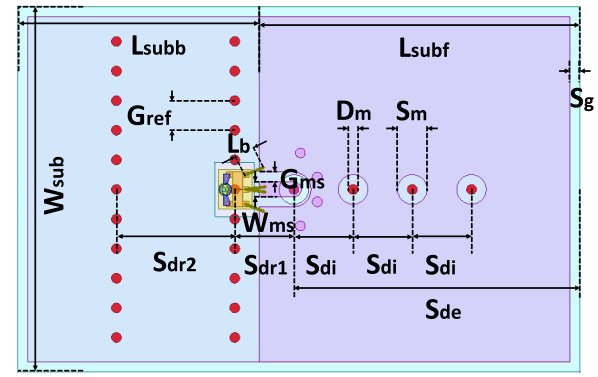
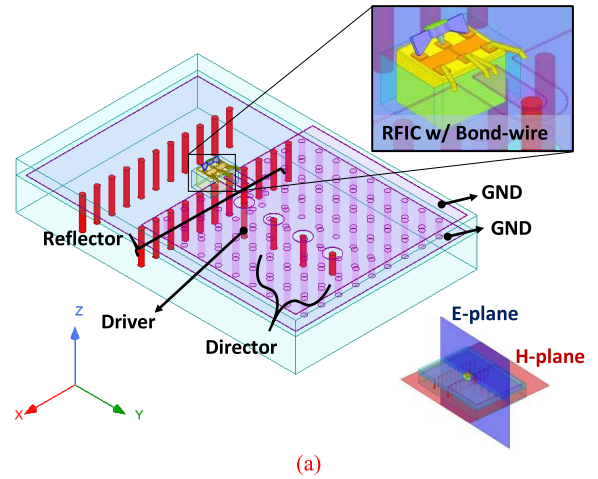


FIGURE 2. Proposed compact vertically polarized end-fire monopole-based Yagi antenna. (a) side view, (b) top view, (c) sectional view.

TABLE 1. Dimensions for proposed antenna.

| Parameter | Value (mm) | Parameter | Value (mm) |
|------------|------------|------------|------------|
| L_{subb} | 2.4 | h_{dir1} | 0.5 |
| L_{subf} | 3.3 | h_{dir2} | 0.35 |
| W_{sub} | 3.7 | h_{ref} | 0.65 |
| t_{cpw} | 0.3 | S_{dir1} | 0.7 |
| t_{rad} | 0.65 | S_{dir2} | 1.1 |
| h_{drv} | 0.6 | S_{di} | 0.6 |
| D_m | 0.1 | S_m | 0.3 |
| W_{ms} | 0.15 | G_{ms} | 0.1 |
| L_b | 0.2 | S_g | 0.1 |
| G_{ref} | 0.3 | t_{ag} | 0.01 |
| S_{de} | 2.9 | | |

method by flipping and attaching the antenna to the base PCB after connecting RFIC with bond wires to the antenna.

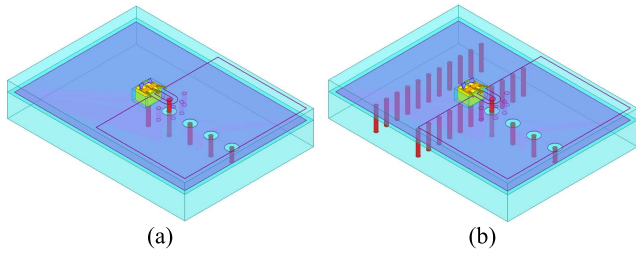


FIGURE 3. Geometry of the proposed antenna (a) with single reflector post and (b) with reflector post array.

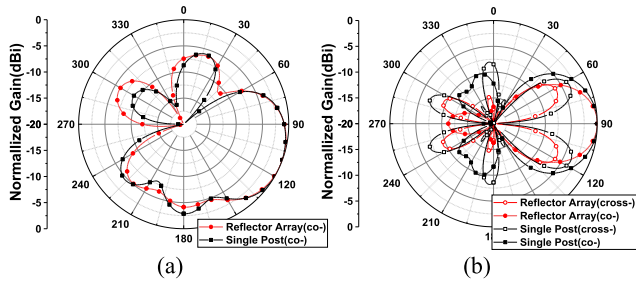


FIGURE 4. Simulated (a) E- and (b) H- normalized radiation pattern of the proposed antenna at 63GHz for the single reflector post and reflector array case.

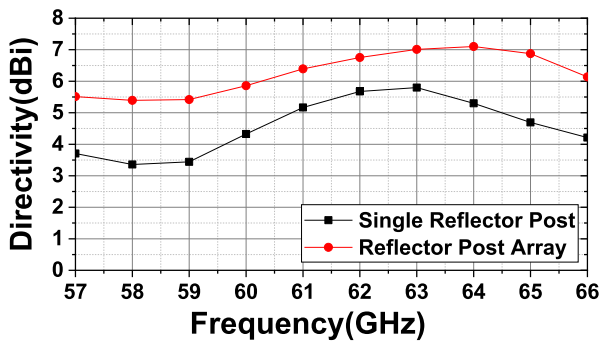


FIGURE 5. Simulated directivity toward end-fire direction (a) single reflector post and (b) reflector post array.

Therefore, it is possible to implement an antenna that is compact and does not interfere with RFIC.

The paper is described below. In section II, the proposed antenna is described. In section III, the simulated and measured performance of the proposed antenna is presented, and this paper is concluded in section IV.

II. ANTENNA DESIGN

A. ANTENNA GEOMETRY

Fig. 2 shows the proposed compact vertically polarized end-fire monopole-based Yagi antenna. The ground-signal-ground(G-S-G) pad is placed at the antenna feeding to make contact from G-S-G probe for antenna measurement. A reflector array and director are arranged to increase the directivity of the antenna. A ground plane is placed on the upper surface of the monopole antenna to reduce the substrate thickness by using the image effect of the monopole.

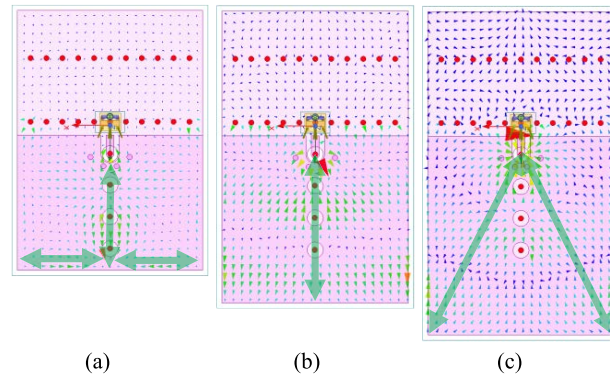


FIGURE 6. Simulated current distribution when sweeping 'Sde' at 63GHz. (a) 2.3mm (b) 2.9mm and (c) 3.5mm case.

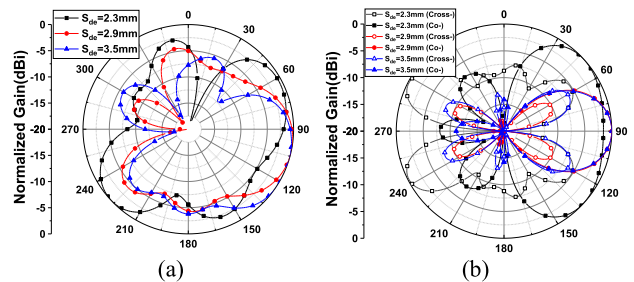


FIGURE 7. Simulated (a) E- and (b) H- normalized radiation pattern at 63GHz when sweeping 'Sde'.

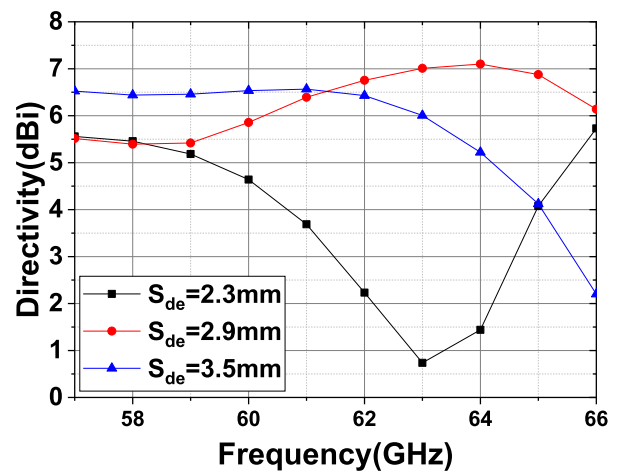


FIGURE 8. Simulated directivity toward end-fire direction when sweeping value 'Sde'.

In order to minimize the length of bond-wire between the antenna and RFIC, a cavity was formed in the upper part of the LTCC so that the RFIC could be inserted into the cavity. Due to the ground plane located under RFIC, the antenna with a monopole radiator does not require a balun, resulting in less loss due to a short feeding line.

The driver, director, and reflector array of the proposed antenna are constructed by placing metal vias of the laminated substrate vertically. The advantage of an antenna structure is that 1) signal loss is minimized due to short

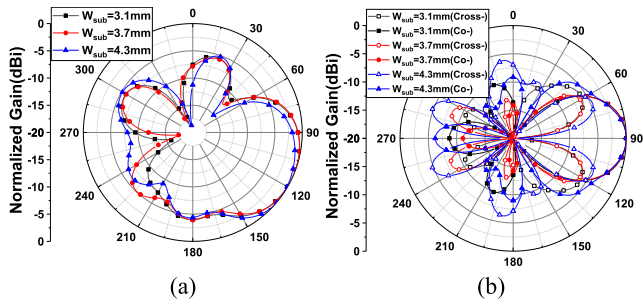


FIGURE 9. Simulated (a) E- and (b) H-normalized radiation pattern of the proposed antenna at 63GHz when sweeping W_{sub} .

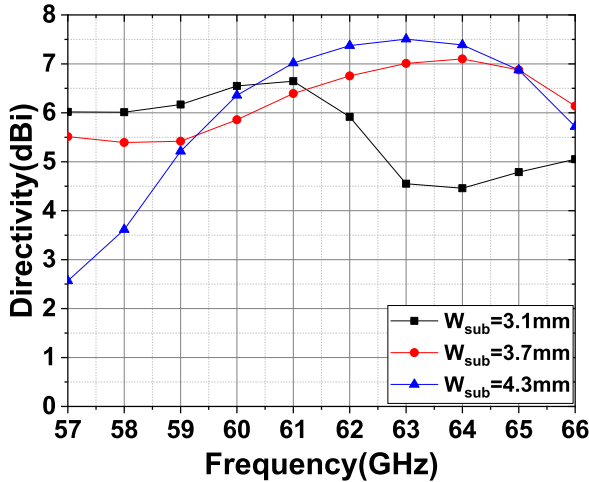


FIGURE 10. Simulated directivity toward end-fire direction when sweeping value ' W_{sub} '.

bond-wire length and 2) a compact AiP can be realized by minimizing the volume of the antenna.

Unlike the conventional Yagi antenna, the proposed monopole-based Yagi-Uda antenna has a ground on the upper surface of the monopole and is not exposed to the air, so the distortion of the radiation pattern is relatively low due to the electrical component placed around the antenna.

The proposed antenna was designed with a LTCC process built-in 16-layer stack up, which comprises 50- μm thick substrates and a 10- μm thick silver layer. The dielectric permittivity (ϵ_r) of the LTCC substrate is 5.9, and the loss tangent is 0.0035 at 60GHz. The overall size of the proposed antenna is designed to be 3.7 x 5.7 x 0.65 mm³. The proposed antenna is simulated using a 3-D full-wave simulator Ansys HFSS. Table 1 shows the dimension for the proposed antenna.

The proposed antenna is designed with the following electrical length. The length of the driver of the antenna is $0.2\lambda_{eff}$ which is slightly smaller than $0.25\lambda_{eff}$. The reflector is slightly longer than the driver, which is $0.22\lambda_{eff}$. The director is used $0.17\lambda_{eff}$, which is slightly shorter than the driver.

Considering the upper part of the LTCC considering RFIC packaging, the overall thickness corresponds to 0.95mm.

B. REFLECTOR DESIGN

Since the proposed antenna is basically realized in LTCC substrate which dielectric constant is as high as 5.9, this

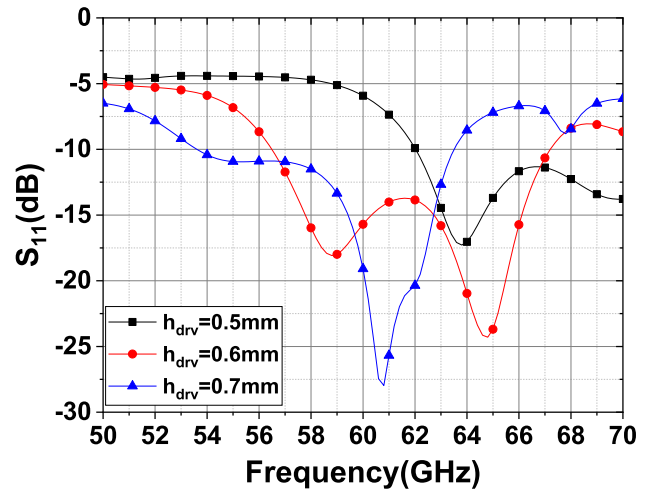


FIGURE 11. Simulated S_{11} when sweeping value ' h_{drv} '.

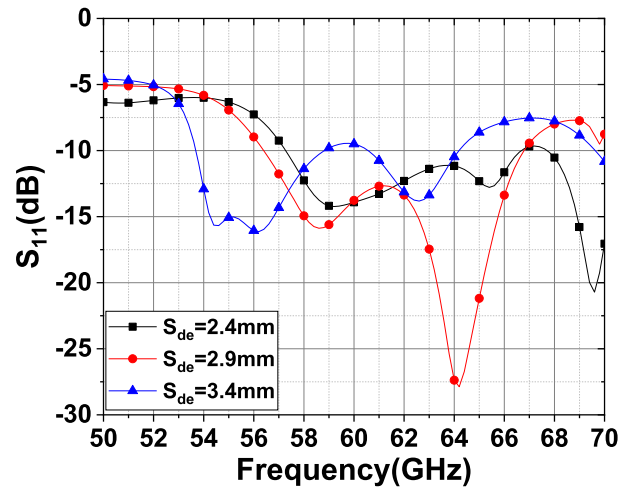


FIGURE 12. Simulated S_{11} when sweeping value ' S_{de} '.

greatly affects the radiation performance. The reflector of the proposed antenna is very important to have end-fire radiation to the front of the antenna by blocking backside radiation with an inductive component. However, in the case of the proposed antenna implemented in the dielectric, it is difficult to prevent backside radiation distributed throughout the dielectric with a single reflector because energy is confined into the dielectric. Fig. 3 shows the geometry of the proposed antenna with single reflector post and with reflector post array. Fig. 4 shows the simulated E- and H-normalized radiation pattern of the proposed antenna at 63GHz for the single reflector post and reflector array case. In case of the single reflector post case, a lot of side lobes are formed due to the surface current, but the radiation pattern radiates evenly toward end-fire direction in the presence of the reflector post array. When reflector post array is placed, the side-lobe and cross-polarization become lower than that of single post case.

Fig. 5 shows the simulated directivity toward end-fire direction in case of single reflector post and reflector post array. In case of the single reflector post, it is shown that

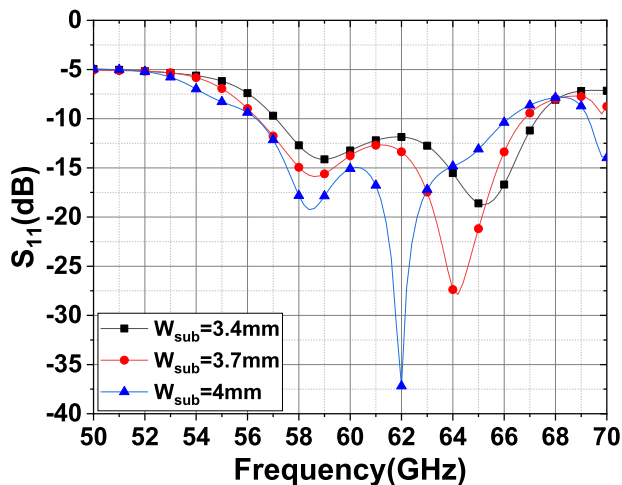


FIGURE 13. Simulated S11 when sweeping value 'Wsub'.

overall directivity is lower than that of the reflector post array. That's because, the directivity of the antenna is decreased due to the multiple side lobes caused by the surface wave. In this work, the directivity is increased by adding reflector post array which suppress the surface wave as much as possible and minimize the side-lobe of the antenna. The front to back ratio of the proposed antenna is increased as well.

C. EFFECT OF THE SUBSTRATE AND GROUND STRUCTURE

Fig. 6 shows the simulated current distribution when sweeping 'S_{de}' at 63GHz. It is shown that the length is equivalent to 1λ_{eff} when 'S_{de}' is set to 2.9mm from the current distribution. In this case, the current generated in the x-direction is minimized because the current resonates in the y-direction. In the case of other frequencies, it is seen that the x-direction current is formed as well since they resonate in the diagonal direction.

Fig. 7 shows the simulated E- and H- normalized radiation pattern when sweeping 'S_{de}' at 63GHz. In case 'S_{de}' is set to 2.9mm, even radiation pattern for the end-fire direction is achieved because the current distribution for the x- component is minimized. However, in case 'S_{de}' is set to 2.3mm or 3.5mm, the radiation pattern is distorted since the current distribution for x-direction is formed. When 'S_{de}' is 2.9mm, the side-lobe is the lowest in E-plane and H-plane and cross-polarization is low compared to other conditions.

Fig. 8 shows simulated directivity toward the end-fire direction when sweeping value 'S_{de}'. In fact, the radiation pattern is distorted except that 'S_{de}' is selected to 2.9mm due to these resonant components in the x-direction, and the directivity in the end-fire direction in a given bandwidth also tends to decrease remarkably at a specific frequency. In this work, 'S_{de}' is set to 2.9mm to obtain a consistent radiation pattern within a given bandwidth.

Fig. 9 shows the simulated E- and H- normalized radiation pattern of the proposed antenna at 63GHz when sweeping W_{sub}. Assuming that 2.9mm is a length equivalent to 1λ_{eff}, 3.1mm, 3.7mm and 4.3mm length corresponds to 1.06 λ_{eff},

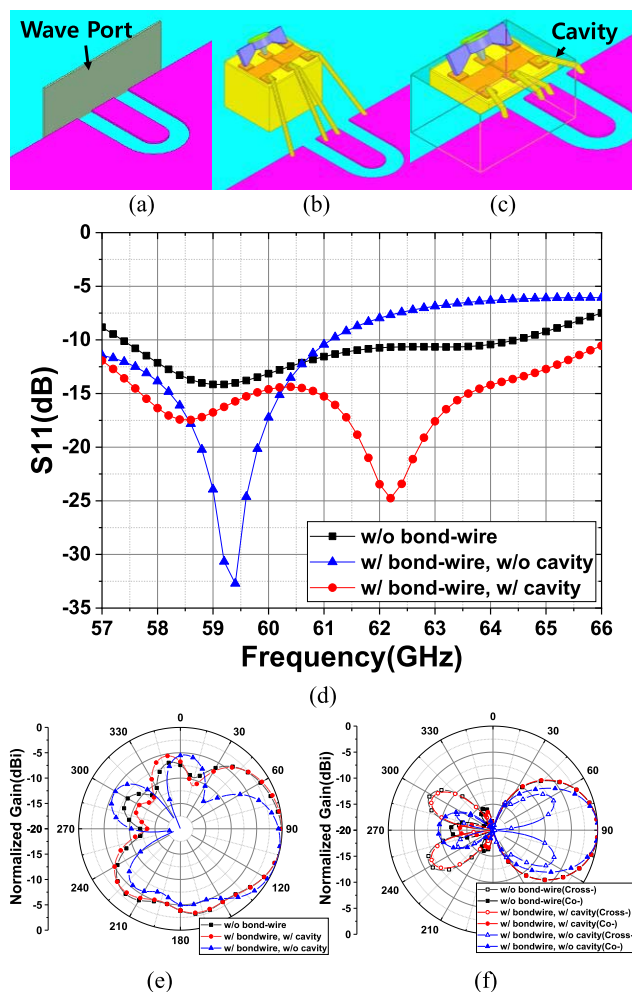


FIGURE 14. Antenna performance comparison with and without cavity. (a) geometry of the proposed antenna without bond-wire (b) geometry of the proposed antenna without cavity (c) geometry of the proposed antenna with cavity, (d) S11 and (e) E-plane and (f) H-plane normalized radiation pattern.

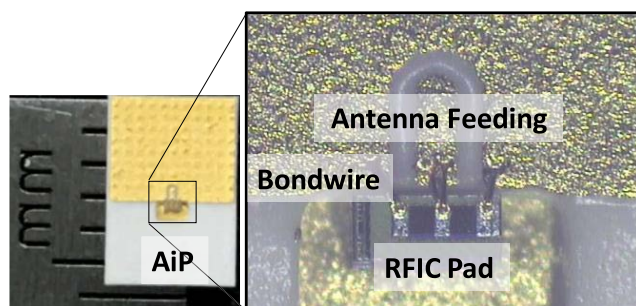


FIGURE 15. Fabricated vertical Yagi-Uda antenna. The proposed antenna is connected with CMOS pad via bond-wire.

1.27λ_{eff} and 1.48 λ_{eff}, respectively. Therefore, in the case of 3.1mm and 4.3mm, resonance toward x-direction occurs and the radiation pattern is also distorted due to the excessive formation of the side-lobes. On the other hand, when the 'W_{sub}' is set to 3.7mm, it can be confirmed that the x-direction resonance is minimized and most of the radiation is concentrated

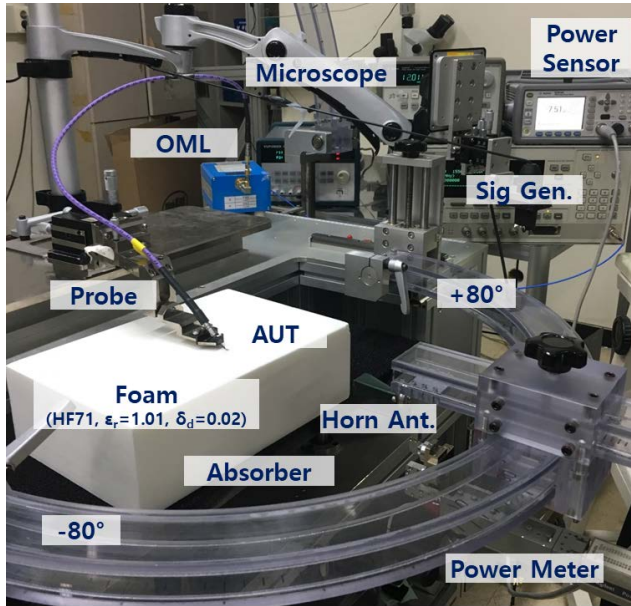


FIGURE 16. Radiation pattern measurement setup for proposed antenna.

in the end-fire direction. Fig. 10 shows the simulated directivity toward the end-fire direction when sweeping value ‘ W_{sub} ’. If the ‘ W_{sub} ’ is not 3.7mm, it is shown that the directivity is remarkably reduced at a certain frequency. Therefore, ‘ W_{sub} ’ was determined to be 3.7mm to allow constant radiation in the end-fire direction over the entire band(57-66GHz).

D. IMPEDANCE ANALYSIS FOR THE PROPOSED ANTENNA

In order to match the input impedance to 50-ohm, it is necessary to make an imaginary impedance to zero. Therefore, it is necessary to find the variables that control the imaginary impedance. When ‘ W_{sub} ’ is 3.7mm, the side-lobe is the lowest in E-plane and H-plane and cross-polarization is low compared to other conditions.

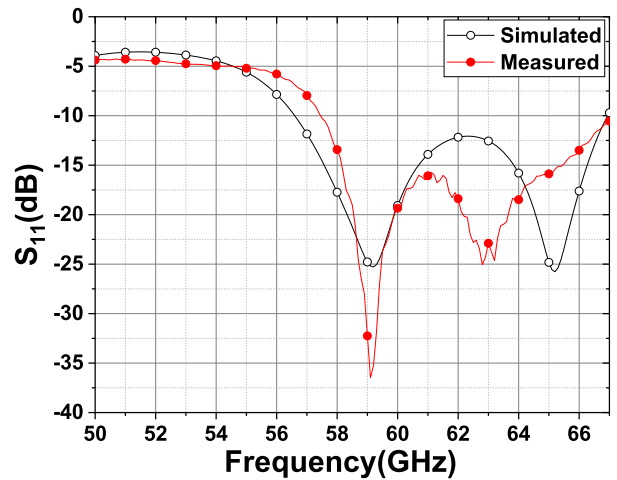
Fig. 11 shows the simulated S_{11} when sweeping value ‘ h_{drv} ’. From the graph, it is seen that the overall resonant frequency decreases as ‘ h_{drv} ’ increases. The length of the driver(=0.6mm) is designed at approximately $0.2 \lambda_{eff}$ for the 60-GHz frequency. Considering the fringing effect and image effect, it can be confirmed that it corresponds to the half-wave resonance.

Fig. 12 shows the simulated S_{11} when sweeping value ‘ S_{de} ’. Since the dielectric constant of the dielectric is as high as 5.9, the resonance characteristic of the dielectric also plays an important role in matching the antenna impedance.

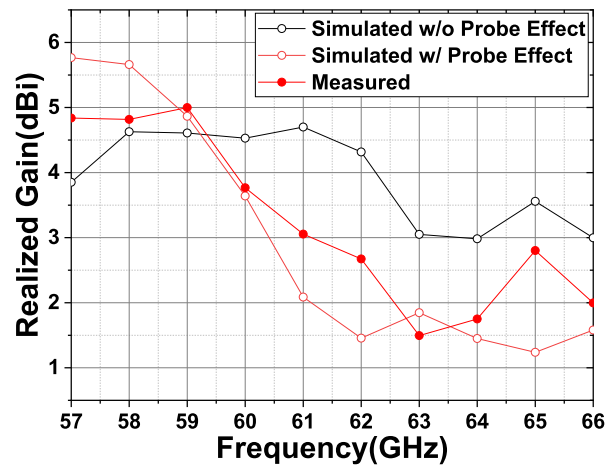
From the graph, it is seen that the overall resonant frequency decreases as ‘ S_{de} ’ increases. In this work, ‘ S_{de} ’ is designed to be 2.9mm corresponding to $1 \lambda_{eff}$.

Fig. 13 shows the simulated S_{11} when sweeping value ‘ W_{sub} ’. It is shown that the second resonance frequency is increased by lowering the width of the substrate.

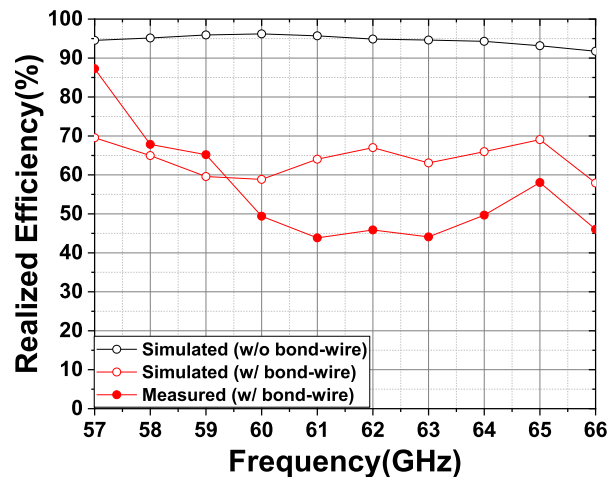
Therefore, it is concluded that the overall resonance frequency is determined by the length of the driver and the space between the driver to the edge of the substrate, and



(a)



(b)



(c)

FIGURE 17. Simulated and measured results; (a) S_{11} with bond-wire interconnect, (b) realized gain included probe and dielectric foam and (c) radiation efficiency.

the second resonance point can be controlled by the size of the ground plane. Using this phenomenon, the antenna was designed by adjusting the second resonant frequency to obtain

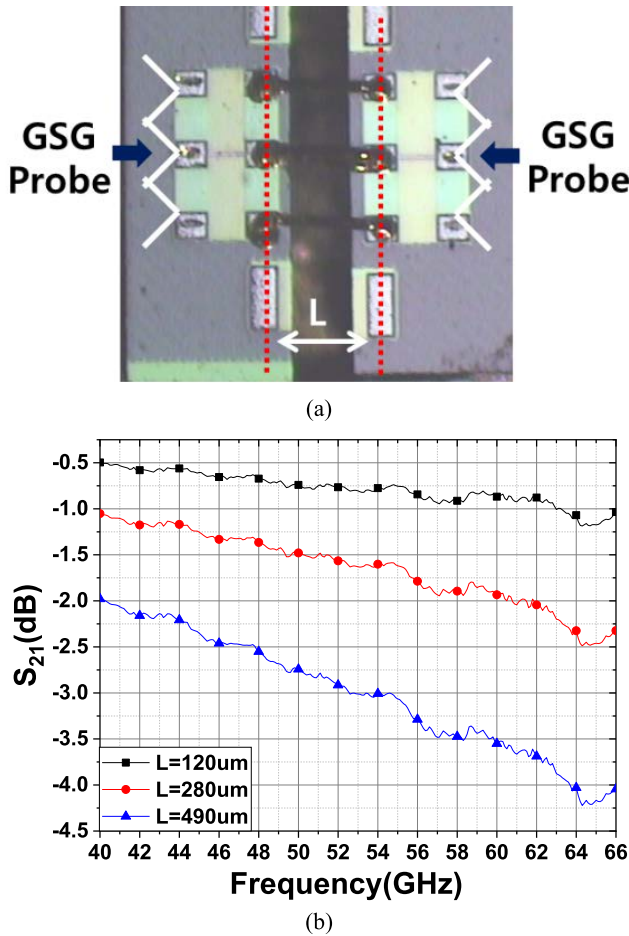


FIGURE 18. Measured insertion loss of bond-wire with CMOS microstrip line; (a) measurement setup and (b) measured insertion loss with varying wire length.

the broadband characteristics and adjusting the remaining parameters to match the center frequency. Fig. 14 shows the antenna performance comparison with and without cavity and with and without bond-wire.

In case of actual use for antenna-in-package, a connection with an RFIC must be considered, and it is interconnected primarily using bond-wire. In a general case, the matching is significantly distorted due to the inductance of the bond-wire. In this work, a cavity was added as much as the height of the RFIC chip to reduce the added inductance by reducing the length of the bond-wire.

In the case with cavity, the length of the bond-wire correspond to $200\mu\text{m}$, and the length of the bond-wire is as long as $500\mu\text{m}$ in the case without cavity due to the mismatch of the height of the antenna and the RFIC.

Since the inductance by the bond-wire is about 1 nH/mm , the impedance deterioration is caused by the additional bond-wire. The S_{11} only covers from 57GHz to 61.1GHz in case without cavity, and the realized efficiency is degraded up to -7.2dB ($=19\%$) in the absence of the cavity for the 60-GHz ISM band. In addition, since radiation occurs in the bond-wire, the antenna radiation characteristic is also severely

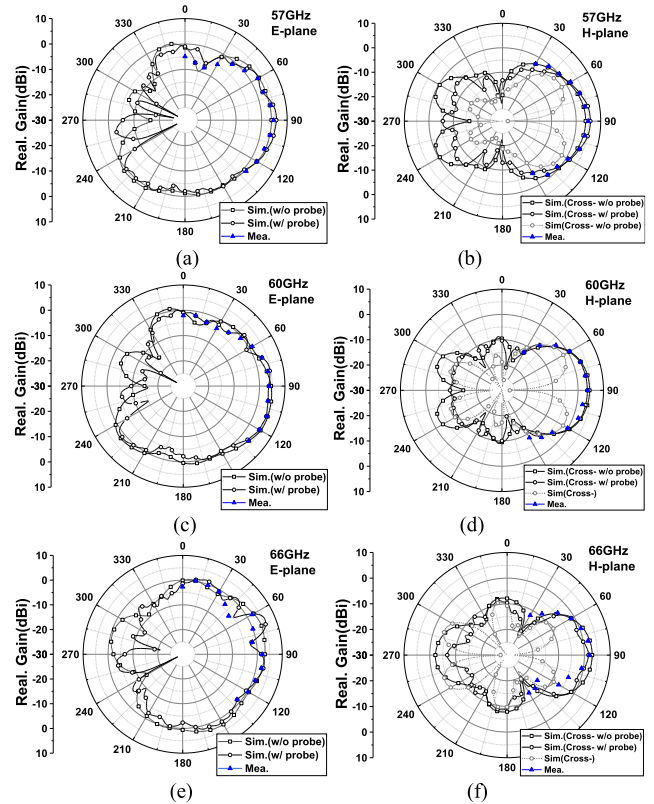


FIGURE 19. Simulated and measured radiation patterns; (a) 57GHz E-plane, (b) 57GHz H-plane, (c) 60GHz E-plane, (d) 60GHz H-plane, (e) 60GHz E-plane and (f) 60GHz H-plane.

TABLE 2. Summary of simulated and measured antenna specifications.

| | Simulated | Measured |
|-----------------------|--|---|
| Peak Gain (57 GHz) | w Probe 5.76 dBi / wo Probe 3.85 dBi | 4.83 dBi |
| E-Plane HPBW (60 GHz) | w Probe : 67° (68° - 135°) / wo Probe : 65° (75° - 140°) | 70° (65° - 135°) |
| H-Plane HPBW (60 GHz) | w Probe : 50° (65° - 115°) / wo Probe : 54° (63° - 117°) | 50° (60° - 115°) |

deteriorated. A cavity was added to prevent deterioration of the radiation pattern by the bond-wire. In fact, in the absence of a cavity, the E-plane radiates in a direction deviating from the boresight direction, and a symmetrical radiation pattern cannot be obtained. In addition, it was confirmed that the 4dB back radiation was improved in the H-plane compared to the case without a cavity.

III. ANTENNA MEASUREMENT

Fig.15 shows the fabricated proposed antenna using LTCC process. The antenna is connected using CMOS GSG pad and bond wires for measurement using the probe.

The thickness of CMOS chip including GSG pad is 0.3mm . In order to reduce the signal insertion loss, the height of the GSG pad of chip is lowered by placing the cavity inside the antenna to make that the top layer of the antenna and the pad is placed in the same height. Fig. 16 shows an radiation pattern

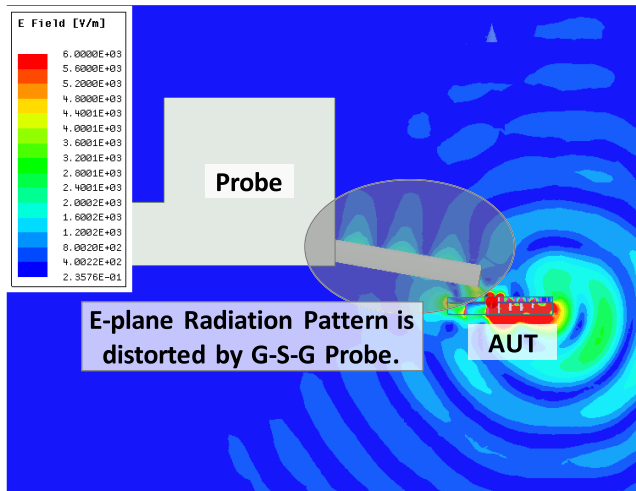


FIGURE 20. Simulated E-field distribution with metal probe.

TABLE 3. Comparison with reported vertical polarized end-fire antennas.

| Ref. | Freq. (GHz) | S ₁₁ BW (GHz) | Peak Gain (dBi) | Antenna Size (λ ₀) | Package (RFIC) |
|-----------|-------------|--------------------------|---|--|----------------|
| [19] | 60 | 25.6 (=39.4%) | 6 ⁽¹⁾ | 0.57 x 0.71x0.43 | N/A |
| [21] | 60 | 7 (=11.6%) | 6 ⁽¹⁾ | 0.96 x 1.28x0.2 | wire-bonding |
| [22] | 39 | 7 (=20%) | 11 ⁽¹⁾ | 2.3 x 4.4x0.17 | N/A |
| [23] | 39 | 3.8 (=9.7%) | 2.8 ⁽¹⁾ | 0.88 x 0.29x0.15 | N/A |
| This work | 60 | 9.6 (=16%) | 6.6 ⁽¹⁾ 4.99 ⁽²⁾ | 0.74 x 1.14 (⁽³⁾ x0.15 ⁽⁴⁾) | wire-bonding |

(1) w/o bond-wires, (2) w/ bond-wires, (3) include RFIC, (4) core height

measurement setup for proposed antenna. The signal from the signal generator is used to generate a 60 GHz frequency signal using OML mixer, and this signal flows through a GSG probe for feeding. A compact microscope is installed for the probing connection, and the antenna radiation pattern is measured using a reference horn antenna while maintaining a constant distance and changing the angle. The signal power value received by the horn antenna can be read through the power sensor and meter. In order to precise measurement, the proposed antenna needs a space for radiation toward downward direction. To secure radiation space, measurement is performed using Rohacell’s HF71 dielectric foam with a permittivity equal to one as air [20]. All measurement results are measured through GSG probing after connecting the CMOS pad with bond wires. Fig. 17(a) shows the result of the simulated and measured input impedance of the proposed antenna connecting CMOS pad by bond-wires. The -10dB impedance bandwidth covers from 57.4 GHz to 67 GHz for the measured case, and it can be seen that the simulation result agrees with the measured result.

It is shown that the first simulated resonance agree well with the measured result at 59 GHz, but the measured second

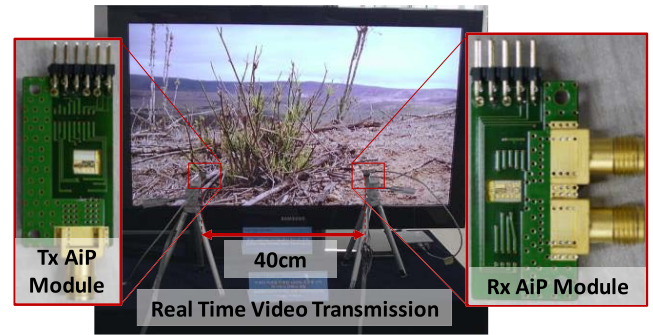


FIGURE 21. Demonstration for real time video-transmission using AiP module.

resonance shifts down to near 63 GHz from the simulated second resonance near 65 GHz. This is minor difference since the simulated and measured S₁₁ level is below -10dB. It is presumed that the cause is a manufacturing error of the cavity or the real value of the dielectric constant of the RFIC inserted into the cavity is different to that of simulated one. Fig. 17(b) shows the peak realized gain of the proposed antenna. The simulation result considering only antenna excluding the probing effect is indicated by a dotted line. The result shows the peak gain of 4.99dBi with 3.5dB fluctuation within the range of the 57-66GHz frequency band. However, the gain fluctuation of the simulated and measured results considering the probe is increased compared to the case without the probe. That’s because the probe is located nearby antenna, and resulting in distortion of the radiation pattern. Since the simulated and the measured results considering both the probe and CMOS pad agree well, it can be predicted that the simulated and measured results excluding the probe effect are similar. Fig. 17(c) shows the simulated radiation efficiency of the proposed antenna. The radiation efficiency applied only to the antenna shows more than 90% in the 57 - 66 GHz band, and the radiation efficiency is decreased to 60% when the antenna is connected to CMOS pad using a bond-wire interconnect. As shown in Fig. 18, when a signal is excited to the antenna, 1.5dB insertion loss occurs due to bond-wire and CMOS pad. Therefore, it is concluded that the radiation efficiency including the corresponding loss value has 20- 30% lower than the result of considering only the antenna. The radiation pattern is measured for the fabricated antenna using the measurement setup. All radiation pattern results are shown in Fig. 19 as including CMOS pads and bond wires. The measured radiation pattern results are distorted and uneven due to the influence of the probe. However, since the simulation results including the probe and the measurement results are almost identical, it is predicted that a even radiation pattern result can be obtained if the probe is removed. The simulated and measured radiation pattern results are summarized in Table 2.

The radiation pattern measurement results indicate that the radiation pattern is severely distorted, especially in E-plane. This is because the probe tip, which is inevitably inserted for antenna radiation measurement, is made of metal and affects radiation. The polarization of the proposed antenna

is formed in the vertical direction of the antenna, so that the direction in which E-field is strongly formed and the direction in which the probe is located coincide, resulting in more severe distortion. In addition, due to characteristics of small height aperture which is in a thin substrate, the beam width is formed wide in the vertical direction, so the effect of the probe is more affected.

Fig. 20 shows the distribution of the simulated E-field in a vertical cross-section. As mentioned above, because the probe is located in the E-plane direction, so E-plane radiation pattern is distorted by reflected from the G-S-G probe. Since the probe located in the vertical direction of the antenna is not used for actual use, it is predicted that a uniform radiation pattern without fluctuation is obtained from the proposed antenna without the G-S-G probe.

Table 3 shows a comparison table of the reported vertically polarized end-fire antenna for the mm-Wave frequency band. Although bond-wire effect interconnection isn't considered for the reported antenna and only presents the performance of the antenna itself, peak gain with and without bond-wire interconnection is presented for the proposed antenna in this work.

Compared to the reported work, the proposed antenna has the lowest thickness thanks to the image effect applied to the monopole antenna. In addition, since all radiating elements are inserted in the dielectric, the proposed AiP has a small area compared to that of other antennas. Therefore, the proposed AiP considered integration with RFIC is suitable for mobile devices due to its compact size.

IV. DEMONSTRATION FOR REAL-TIME VIDEO TRANSMISSION USING AiP MODULE

Fig. 21 shows the demonstration for real time video-transmission using AiP module. The 1080i HD video signal which corresponds to 1.5Gbps is transmitted by Tx and Rx AiP module. Thanks to the compact size of the proposed AiP, overall size of the Tx and Rx AiP module is as small as $15.7 \times 32\text{mm}^2$ and $17 \times 32\text{mm}^2$, respectively. Tx and Rx module is realized using transceiver reported in [2], and real-time video transmission is successfully demonstrated using OOK modulation with the transmission distance of 40cm.

V. CONCLUSION

In this work, wideband, compact vertically polarized end-fire monopole-based Yagi antenna-in-package is proposed for 60GHz band. The size of the antenna is reduced thanks to the image effect by placing the antenna as a monopole structure. The proposed antenna is interconnected with CMOS chip via a bond-wire interconnect. The realized peak gain of the proposed antenna is 4.99dBi and S_{11} bandwidth is 9.6GHz (57.4GHz-67GHz) which corresponds to 16% fractional bandwidth. The total volume of the antenna is as small as $0.74 \times 1.14 \times 0.15\lambda_0^3$.

REFERENCES

[1] *FCC Rules for 60 GHz Operation*, document CFR 47 15.255, 2010.

- [2] C. W. Byeon, C. H. Yoon, and C. S. Park, "A 67-mW 10.7-Gb/s 60-GHz OOK CMOS transceiver for short-range wireless communications," *IEEE Trans. Microw. Theory Techn.*, vol. 61, no. 9, pp. 3391–3401, Aug. 2013.
- [3] K. Okada et al., "A 64-QAM 60GHz CMOS transceiver with 4-channel bonding," in *IEEE Int. Solid-State Circuits Conf. (ISSCC) Dig. Tech. Papers*, Feb. 2014, pp. 346–347.
- [4] M. Boers et al., "A 16TX/16RX 60 GHz 802.11ad chipset with single coaxial interface and polarization diversity," in *IEEE Int. Solid-State Circuits Conf. (ISSCC) Dig. Tech. Papers*, Feb. 2014, pp. 344–345.
- [5] R. Wu et al., "A 42 Gb/s 60 GHz CMOS transceiver for IEEE 802.11ay," in *IEEE Int. Solid-State Circuits Conf. (ISSCC) Dig. Tech. Papers*, Jan. 2016, pp. 248–249.
- [6] A. Rashidian, S. Jafarlou, A. Tomkins, K. Law, M. Tazlauanu, and K. Hayashi, "Compact 60 GHz phased-array antennas with enhanced radiation properties in flip-chip BGA packages," *IEEE Trans. Antennas Propag.*, vol. 67, no. 3, pp. 1605–1619, Mar. 2019.
- [7] H. Y. Kim, T. H. Jang, H. H. Bae, and C. S. Park, "A 60 GHz compact multidirectional-beam antenna-in-package for mobile devices," *IEEE Antennas Wireless Propag. Lett.*, vol. 18, no. 11, pp. 2434–2438, Nov. 2019.
- [8] W. Hong, K.-H. Baek, and S. Ko, "Millimeter-wave 5G antennas for smartphones: Overview and experimental demonstration," *IEEE Trans. Antennas Propag.*, vol. 65, no. 12, pp. 6250–6261, Dec. 2017.
- [9] H. Wang, K. E. Kedze, and I. Park, "A high-gain and wideband series-fed angled printed dipole array antenna," *IEEE Trans. Antennas Propag.*, vol. 68, no. 7, pp. 5708–5713, Feb. 2020.
- [10] T. Ma, J. Ai, M. Shen, and W. T. Joines, "Design of novel broadband endfire dipole array antennas," *IEEE Antennas Wireless Propag. Lett.*, vol. 16, pp. 2935–2938, 2017.
- [11] T. H. Jang, H. Y. Kim, and C. S. Park, "A 60 GHz wideband switched-beam dipole-array-fed hybrid horn antenna," *IEEE Antennas Wireless Propag. Lett.*, vol. 17, no. 7, pp. 1344–1348, Jul. 2018.
- [12] X. Cai, W. Geyi, and H. Sun, "A printed dipole array with high gain and endfire radiation," *IEEE Antennas Wireless Propag. Lett.*, vol. 16, pp. 1512–1515, 2017.
- [13] R. A. Alhalabi and G. M. Rebeiz, "High-gain Yagi-Uda antennas for millimeter-wave switched-beam systems," *IEEE Trans. Antennas Propag.*, vol. 57, no. 11, pp. 3672–3676, Nov. 2009.
- [14] H.-C. Huang, J.-C. Lu, and P. Hsu, "On the size reduction of planar Yagi-Uda antenna using parabolic reflector," in *Proc. Asia-Pacific Microw. Conf. (APMC)*, Dec. 2015, pp. 1–3.
- [15] S. Lim and M. F. Iskander, "Design of a dual-band, compact Yagi antenna over an EBG ground plane," *IEEE Antennas Wireless Propag. Lett.*, vol. 8, pp. 88–91, 2009.
- [16] J. Bourqui, M. Okoniewski, and E. C. Fear, "Balanced antipodal Vivaldi antenna with dielectric director for near-field microwave imaging," *IEEE Trans. Antennas Propag.*, vol. 58, no. 7, pp. 2318–2326, Jul. 2010.
- [17] I. Linardou and C. Migliaccio, "Twin Vivaldi antenna for transponders and monopulse systems," *Microw. Opt. Technol. Lett.*, vol. 27, pp. 207–209, Nov. 2000.
- [18] Y. Yang, Y. Wang, and A. E. Fathy, "Design of compact Vivaldi antenna arrays for UWB see through wall applications," *Prog. Electromagn. Res.*, vol. 82, pp. 401–418, 2008.
- [19] Y. Li and K.-M. Luk, "A multibeam end-fire magnetoelectric dipole antenna array for millimeter-wave applications," *IEEE Trans. Antennas Propag.*, vol. 64, no. 7, pp. 2894–2904, Jul. 2016.
- [20] K. Iigusa et al., "Gain enhancement of H-Plane sectoral post-wall horn antenna by connecting tapered slots for millimeter-wave communication," *IEEE Trans. Antennas Propag.*, vol. 60, no. 12, pp. 556–5548, Dec. 2011.
- [21] R. Suga, H. Nakano, Y. Hirachi, J. Hirokawa, and M. Ando, "Cost-effective 60-GHz antenna package with end-fire radiation for wireless file-transfer system," *IEEE Trans. Microw. Theory Techn.*, vol. 58, no. 12, pp. 3989–3995, Dec. 2010.
- [22] L. Wang, M. Esquius-Morote, H. Qi, X. Yin, and J. R. Mosig, "Phase corrected H-plane horn antenna in gap SIW technology," *IEEE Trans. Antennas Propag.*, vol. 65, no. 1, pp. 347–353, Jan. 2017.
- [23] J. Park, H. Seong, Y. N. Whang, and W. Hong, "Energy-efficient 5G phased arrays incorporating vertically polarized endfire planar folded slot antenna for mmWave mobile terminals," *IEEE Trans. Antennas Propag.*, vol. 68, no. 1, pp. 230–241, Jan. 2020.
- [24] A. H. Naqvi, J. Park, C. Baek, and S. Lim, "Via-monopole based quasi Yagi-Uda antenna for W-band applications using through glass silicon via (TGSV) technology," *IEEE Access*, vol. 8, pp. 9513–9519, 2020.

- [25] D. C. Nascimento, R. Schildberg, J. C. da, and S. Lacava, "Low-cost Yagi-Uda monopole array," in *Proc. IEEE Antennas Propag. Soc. Int. Symp.*, Jul. 2008, pp. 1–4.



HONGYI KIM received the B.S.E.E. degree from the Department of Electronic and Electrical Engineering, Hong-ik University, Seoul, South Korea, in 2007, and the Ph.D. degree from the Korea Advanced Institute of Science and Technology, Daejeon, South Korea, in 2021. From December 2019 to February 2022, he joined WiseJet Inc., Daejeon, where he was a Senior Design Engineer involved in the development of millimeter-wave RF system and antenna-in-package. Since May 2022, he has been a Senior Engineer with Hanwha Systems, Yongin, Gyeonggi-Do, South Korea. His research interests include design of RF systems, phased arrays, antenna-in-package for radar, and wireless communications applications.



TAE HWAN JANG (Member, IEEE) received the B.S. degree from the Department of Electronic Engineering, Hanyang University, South Korea, in 2014, and received the Ph.D. degree in electronic engineering from the Korea Advanced Institute of Science and Technology (KAIST), Daejeon, South Korea, in 2019. Since 2020, he has been a Staff Researcher with the Samsung Advanced Institute of Technology (SAIT), Suwon, South Korea. His interests include millimeter-wave antenna and CMOS RF circuits and systems. Since 2022, he has been with Hanyang University, Ansan, Gyeonggi-Do, South Korea, where he is an Assistant Professor.



CHUL SOON PARK (Fellow, IEEE) received the B.S. degree from Seoul National University, Seoul, South Korea, in 1980, and the M.S. and Ph.D. degrees in materials science and engineering from the Korea Advanced Institute of Science and Technology (KAIST), Daejeon, South Korea, in 1982 and 1985, respectively. From 1985 to 1999, he worked with the Electronics and Telecommunication Research Institute (ETRI), where he contributed to the development of semiconductor devices and circuits. From 1987 to 1989, he studied the very initial growth of group IV semiconductors during a visit to AT&T Bell Laboratories, Murray Hill, NJ. Since 1999, he has been with the Information and Communications University (which merged with KAIST in 2009), Daejeon, where he is a Full Professor with the Engineering School and the Director of the Intelligent Radio Engineering Center. His research interests include reconfigurable RF integrated circuits (RFICs), millimeter-wave integrated circuits (ICs), and their system-on-chip (SoC)/system-on-package (SoP) integration.

• • •